NASA/TM—1998-208406

Sintering and Creep Behavior of Plasma-Sprayed Zirconia and Hafnia Based Thermal Barrier Coatings

Dongming Zhu
Ohio Aerospace Institute, Cleveland, Ohio

Robert A. Miller
Lewis Research Center, Cleveland, Ohio

Prepared for the
25th International Conference on Metallurgical Coatings and Thin Films
sponsored by the American Vacuum Society
San Diego, California, April 27—May 1, 1998

National Aeronautics and
Space Administration

Lewis Research Center

July 1998

Acknowledgments

The authors are grateful to George W. Leissler for his assistance in the preparation of plasma-sprayed ceramic coating specimens, and to Ralph G. Garlick for performing X-ray diffraction experiments.

Available from

NASA Center for Aerospace Information
7121 Standard Drive
Hanover, MD 21076
Price Code: A03

National Technical Information Service
5287 Port Royal Road
Springfield, VA 22100
Price Code: A03

SINTERING AND CREEP BEHAVIOR OF PLASMA-SPRAYED ZIRCONIA AND HAFNIA BASED THERMAL BARRIER COATINGS

Dongming Zhu † and Robert A. Miller

† Ohio Aerospace Institute

National Aeronautics and Space Administration

Lewis Research Center, Cleveland, OH 44135

ABSTRACT

The sintering and creep of plasma-sprayed ceramic thermal barrier coatings under high temperature conditions are complex phenomena. Changes in thermomechanical and thermophysical properties and in the stress response of these coating systems as a result of the sintering and creep processes are detrimental to coating thermal fatigue resistance and performance. In this paper, the sintering characteristics of ZrO_2-8wt%Y_2O_3, ZrO_2-25wt%CeO_2-2.5wt%Y_2O_3, ZrO_2-6w%NiO-9wt%Y_2O_3, ZrO_2-6wt%Sc_2O_3-2wt%Y_2O_3 and HfO_2-27wt%Y_2O_3 coating materials were investigated using dilatometry. It was found that the HfO_2-Y_2O_3 and baseline ZrO_2-Y_2O_3 exhibited the best sintering resistance, while the NiO-doped ZrO_2-Y_2O_3 showed the highest shrinkage strain rates during the tests. Higher shrinkage strain rates of the coating materials were also observed when the specimens were tested in Ar+5%H_2 as compared to in air. This phenomenon was attributed to an enhanced metal cation interstitial diffusion mechanism under the reducing conditions. It is proposed that increased chemical stability of coating materials will improve the material sintering resistance.

I. INTRODUCTION

Plasma-sprayed ceramic thermal barrier coatings are being developed for advanced gas turbine and diesel engine applications to improve engine reliability and efficiency. Since these coatings are experiencing severe thermomechanical cycling during engine operation, it is especially challenging to develop coating systems with high reliability and durability. In particular, ceramic

Paper presented in *The 25th International Conference on Metallurgical Coatings and Thin Films*, San Diego, California, April 27–May 1, 1998. To be published in Surface and Coatings Technology.

coating sintering and creep at high temperature are among the most important issues for the development of advanced thermal barrier coatings, as has been recognized by many investigators [1-10] . The ceramic sintering and creep at high temperature can result in coating shrinkage and through-thickness cracking during cooling, thereby further accelerating the coating failure process. Sintering-segmentation-enhanced delamination can be an important failure mechanism for a thermal barrier coating system, due to stress concentration from the through-thickness cracks, and increased coating elastic modulus from the sintering densification process. The increase in coating thermal conductivity is also detrimental to coating performance. Research efforts involving various techniques have also been made in characterizing the ceramic coating sintering and creep behavior at high temperature and under temperature gradients simulating those encountered in the engine [1, 2, 7, 11-13] .

The sintering and creep of plasma-sprayed, porous and microcracked ceramic thermal barrier coatings are complex phenomena. The early work by Firestone *et al* [1, 2] indicated that the ceramic creep appeared to be a thermally activated process, with the ceramic splat-sliding being an important creep deformation mechanism. More recently, it has been reported that the ceramic thermal barrier coatings can sinter and creep significantly under compressive stress states at relatively low temperatures [11, 13, 14] . The "creep" of plasma-sprayed ZrO_2-8wt%Y_2O_3 at room temperature has also been observed at a tensile stress of 7.4 MPa [15] . A mechanism-based model has been proposed to describe the densification and deformation occurring in thermal barrier coatings at temperature by taking into account the thermally and stress activated diffusion, and the mechanical compacting processes [13] . The dopants in the ceramic coatings can significantly modify the point defect and microstructures in the bulk, at splat-grain boundaries and microcrack surfaces of the materials, thereby can significantly affect these sintering and creep processes. A better understanding of the dopant effects will help to develop future advanced, sintering/creep resistant "superalloy-type" ceramic coatings.

The purpose of this paper is to investigate sintering kinetics of several zirconia and hafnia based ceramic coating materials. The ceramic materials investigated include: (a) ZrO_2-8wt%Y_2O_3, a NASA-Lewis Research Center reference (or baseline) material; (b) ZrO_2-25wt%CeO_2-2.5wt%Y_2O_3, a commercially available coating material developed for hot corrosion resistance; (c) HfO_2-27wt%Y_2O_3, a potential new coating material developed at NASA for high temperature stability [16] ; (d) ZrO_2-6wt%NiO-9wt%Y_2O_3, a NiO-doped ZrO_2-Y_2O_3 coating material reported to suppress the tetragonal-monoclinic phase transformation [17] ; (e) ZrO_2-6wt%Sc_2O_3-

2wt%Y_2O_3, developed for improved hot corrosion resistance [18] . The coating sintering and creep mechanisms and dopant effect on coating sintering rates are discussed based on experimental observations and possible defect reactions.

II. EXPERIMENTAL MATERIALS AND METHODS

The five ceramic coating materials mentioned above, ZrO_2-8wt%Y_2O_3, ZrO_2-25wt%CeO_2-2.5wt%Y_2O_3, ZrO_2-6wt%NiO-9wt%Y_2O_3, ZrO_2-6wt%Sc_2O_3-2wt%Y_2O_3 and HfO_2-27wt%Y_2O_3, were chosen for this study. The actual compositions of these materials were close to the their nominal compositions. Each of the above materials was prepared by sintering and crushing except for ZrO_2-25CeO_2-2.5wt%Y_2O_3 which was spray dried and plasma spheroidized. A single set of standard plasma-spray parameters was used for each material. The powders with an average particle size of 60 μm of these coating materials were first plasma-sprayed onto 3 mm diameter graphite cylindrical bars, using the plasma spray conditions described previously [19] . The coating thickness was about 0.76 mm, and porosity was about 10%. The graphite bars were then slowly burnt off at 600°C for 6 hours in a furnace in air. The hollow ceramic cylinders were cut into 25.4 mm dilatometer specimens.

Ceramic sintering experiments were carried out in air and in Ar+5%H_2 within the temperature range of 900 to 1400°C, using a UNITHERM™ high temperature dilatometer system shown in Figure 1. Since the push rod in the dilatometer exerts a certain amount of force (measured at approximately 450g using a spring device) on the specimen, a uniaxial stress of

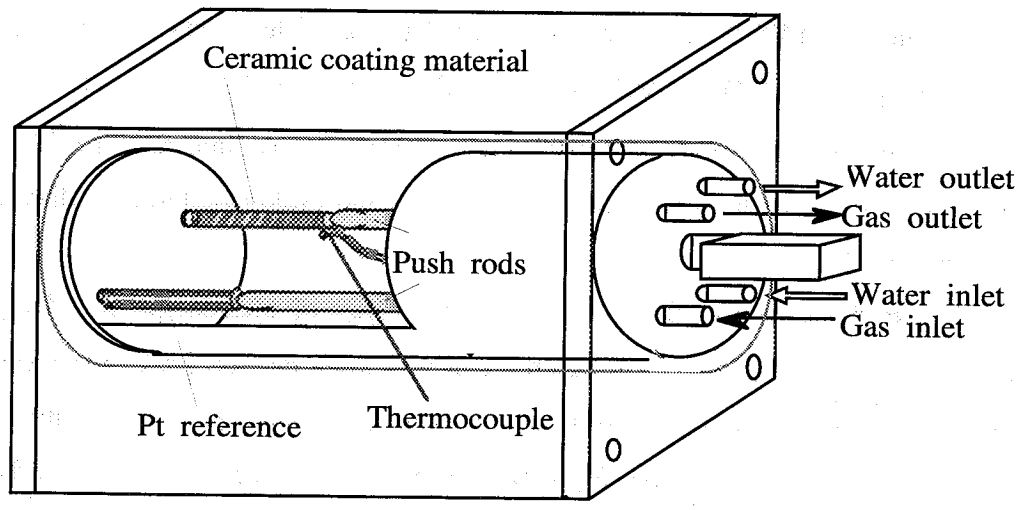

Fig. 1 Schematic diagram showing the ceramic sintering experiment using dilatomentry.

approximately 0.5 MPa was acting on the specimen during the entire sintering test. Therefore, this experiment can also be considered a low constant-stress creep test for the ceramic materials. During the sintering/creep experiments at various test temperatures, all specimens were heated in at rate of 5°C/minute and held at the given test temperature for 15 hours, and then cooled down at a rate of 5°C/minute to room temperature. Specimen shrinkage during the heating/cooling cycles was continuously recorded in a computer system. Surface morphology changes of the specimens due to the sintering process were examined using a scanning electron microscope (SEM). Phase structures of the specimens before and after dilatometer sintering tests were also examined by X-ray diffractometry with Cu K_α radiation.

III. EXPERIMENTAL RESULTS

Figure 2 shows thermal expansion (shrinkage) results for the coating materials during the sintering experiments at various temperatures measured by the dilatometry technique. Sintering shrinkage were observed for all materials when the specimens were held at temperature for 15 hours. The shrinkage strains increased with increasing temperature. It can be seen that the HfO_2-27wt% Y_2O_3 showed the best sintering resistance. In contrast, CeO_2-, Sc_2O_3, and NiO-doped ZrO_2-Y_2O_3 materials exhibit significant sintering shrinkage. Below the temperature of 900°C, no significant shrinkage strains were detected for the given test time. Figure 3 illustrates the sintering shrinkage strains occurring at the isothermal sintering stages as a function of temperature.

The sintering rates of the ceramic materials at the isothermal stages change with time, especially at the early sintering time period. As shown in examples in Figure 4 (a) and (b), faster shrinkage rates were observed initially, however, relatively constant rates were observed for longer sintering times. At 1400°C as shown in Figure 4 (c), the "steady state" sintering rates for ZrO_2-Y_2O_3, ZrO_2-CeO_2-Y_2O_3, ZrO_2-Sc_2O_3-Y_2O_3, ZrO_2-NiO-Y_2O_3, and HfO_2-Y_2O_3 are 2.6×10^{-8} / sec., 3.8×10^{-8} / sec. 4.2×10^{-8} / sec., 8.5×10^{-8} / sec. and 6.4×10^{-9} / sec., respectively. Figure 4 (d) shows that for ZrO_2-NiO-Y_2O_3, the second cycle resulted in further shrinkage of the specimen at 1200°C.

Figure 5 shows the sintering shrinkage kinetics of plasma-sprayed ZrO_2-8wt%Y_2O_3 at 1200°C in air and in Ar+5%H_2. It can be seen that when the specimen was tested in a reducing atmosphere, a faster sintering shrinkage rate was observed. In addition, the ceramic coating material turned black after this Ar+H_2 treatment. Increased sintering rates and darkened color were observed for all other materials under the reduced oxygen partial pressure condition. This may imply that the more defective structure of the materials due to Ar+H_2 sintering would increase the

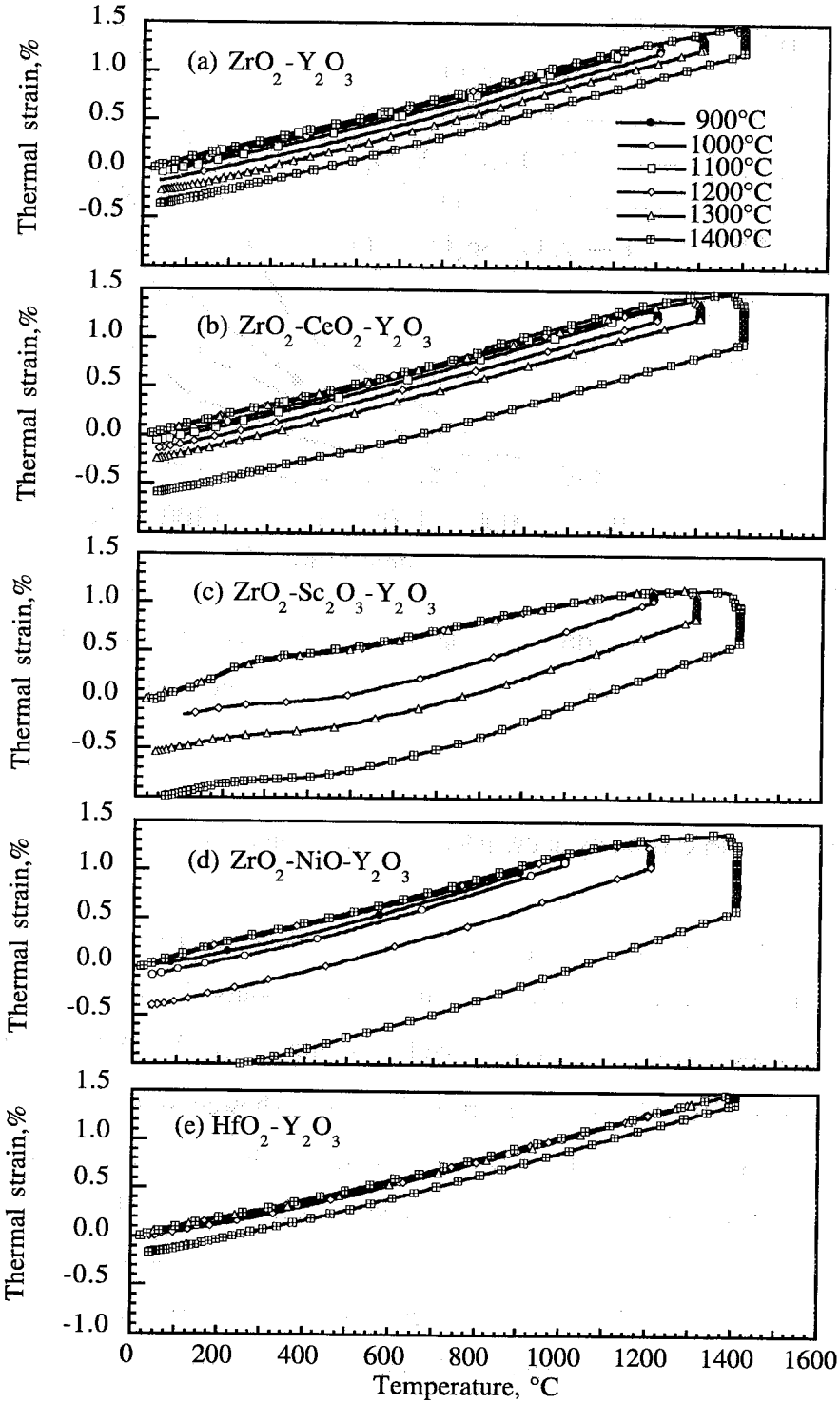

Fig. 2 Thermal expansion and sintering shrinkage response for the coating materials during the dilatometry sintering experiments at various temperatures. (a) ZrO_2-8wt%Y_2O_3; (b) ZrO_2-25wt%CeO_2-2.5wt%Y_2O_3; (c) ZrO_2-6wt%Sc_2O_3-2wt%Y_2O_3; (d) ZrO_2-6wt%NiO-9wt%Y_2O_3; (e) HfO_2-27wt%Y_2O_3.

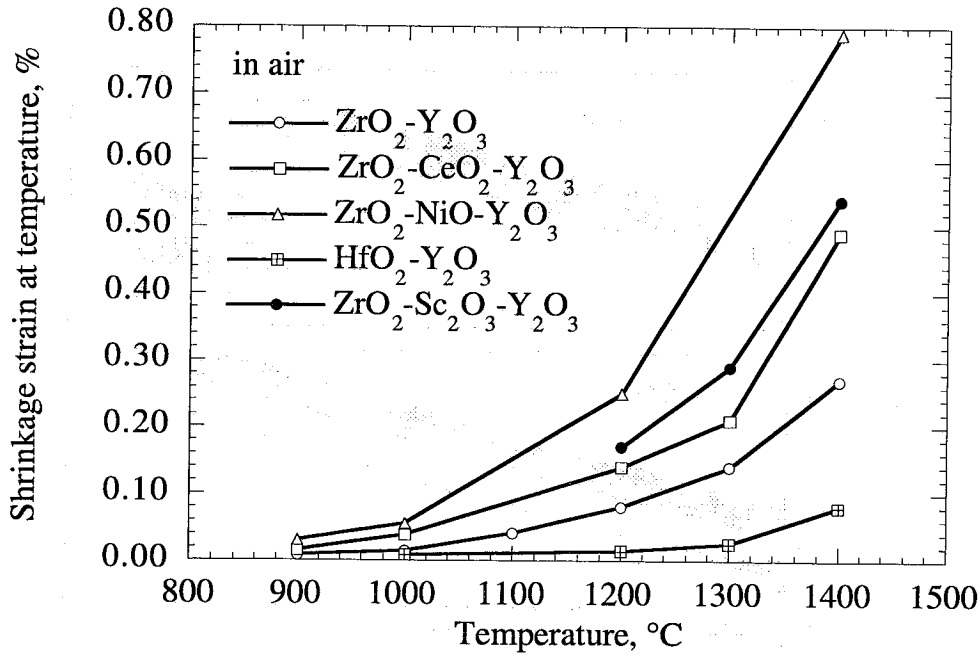

Fig. 3 Total sintering shrinkage strains for the coating materials at the 15 hour isothermal sintering stages as a function of temperature.

minority defect transport especially at the internal surfaces and grain boundaries, thus resulting in a faster sintering rate.

Figure 6 illustrates some examples of the X-ray diffraction spectra for ZrO_2-Y_2O_3, ZrO_2-CeO_2-Y_2O_3, HfO_2-Y_2O_3 and ZrO_2-Sc_2O_3-Y_2O_3 after 15 hours sintering at 1200°C in air. From X-ray diffraction experiments, it was found that the baseline ZrO_2-8wt%Y_2O_3 primarily consisted of tetragonal t' phase. The CeO_2-doped ZrO_2-Y_2O_3 also showed significant amount of t' phase, however, the possibility that the cubic c phase might also be increased as compared to the baseline material requires further study. Due to the high concentration of yttria dopant, HfO_2-27wt%Y_2O_3 had a fully stabilized cubic c phase. No appreciable monoclinic phase was observed in these three materials. Heat treatments related to the sintering experiments under various temperature and oxygen pressure conditions did not measurably alter the phase structures of these materials. The as-sprayed ZrO_2-Sc_2O_3-Y_2O_3 material showed tetragonal t' phase and an increased amount of the monoclinic m phase. The monoclinic phase in the Sc_2O_3-doped materials increased after the sintering tests.

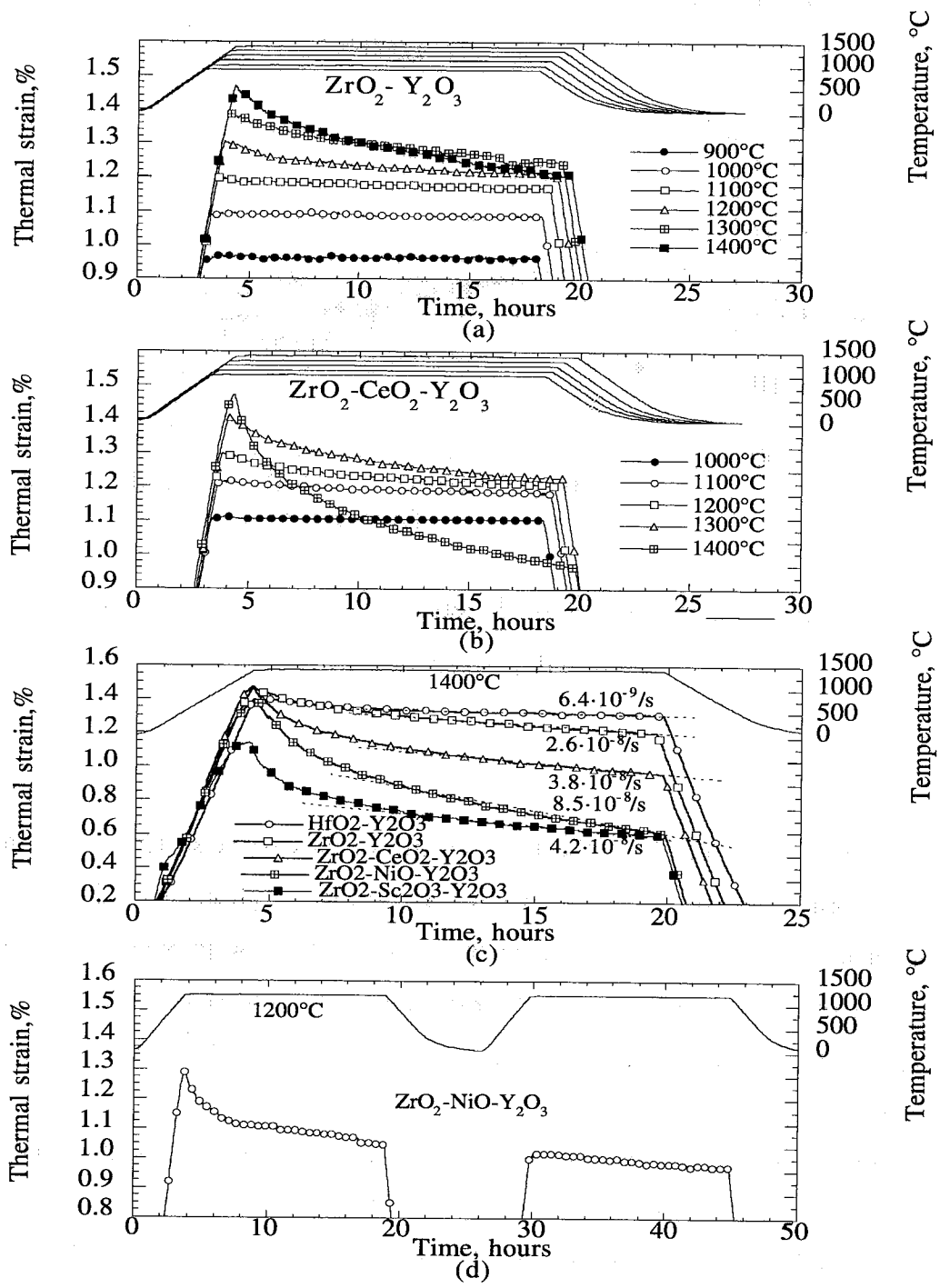

Fig. 4 Sintering behavior of the ceramic materials at the isothermal stages. (a) and (b) The sintering strains as a function of time and temperature for ZrO_2-8wt%Y_2O_3 and ZrO_2-25wt%CeO_2-2.5wt%Y_2O_3, respectively; (c) Steady state creep rates for the ceramic materials at 1400°C; (d) Sintering shrinkage of ZrO_2-6wt%NiO-9wt%Y_2O_3 at 1200°C under two temperature cycles.

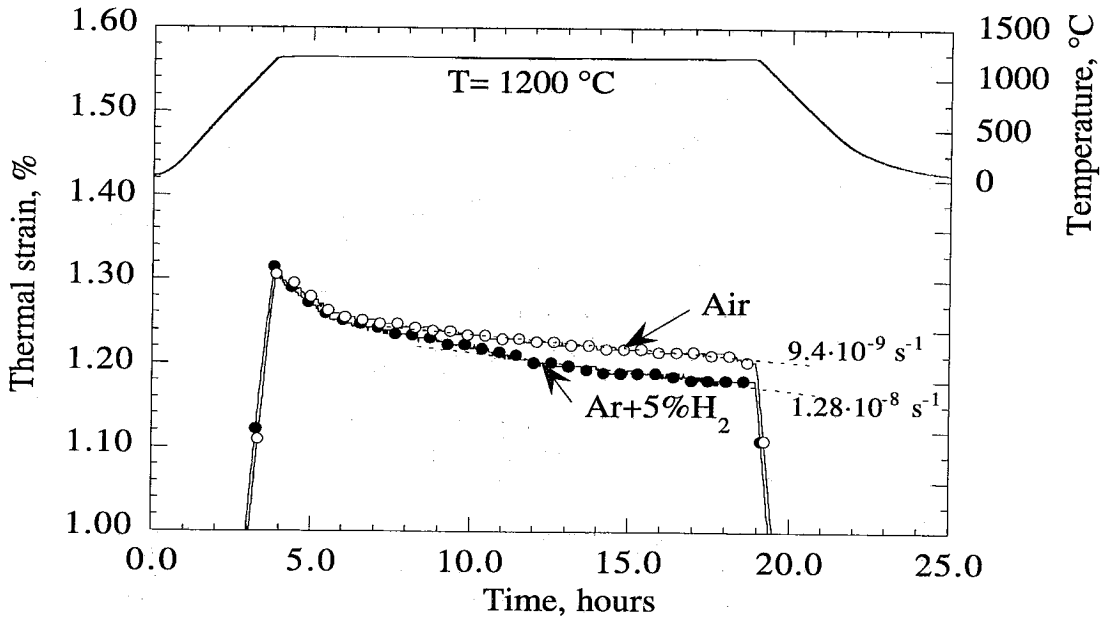

Fig. 5 Sintering shrinkage kinetics of plasma-sprayed ZrO_2-8wt%Y_2O_3 at 1200°C in air and in Ar+5%H_2.

The NiO-doped ZrO_2-Y_2O_3 showed more complex phase structures. As shown in Figure 6, The majority phase in ZrO_2-NiO-Y_2O_3 was the cubic *c* phase, instead of tetragonal phase in the baseline material. However, the monoclinic *m* phase was also present in this material. Because of the limited solubility of NiO in ZrO_2-Y_2O_3 (about 3 mol% at 1600°C [17]), NiO phase was observed in the as-sprayed and air-sintered specimens. In the Ar+H_2 sintered specimens, however, a Ni phase was present because of the reduction of NiO.

Surface microstructure changes were also observed after the sintering experiments. Certain regions showed more noticeable sintering densification and grain growth as compared to other regions, indicating there were some heterogeneities in the observed sintering phenomena. Figure 7 shows micrographs of ceramic surfaces of the ZrO_2-8wt%Y_2O_3 coating material before and after the dilatometry sintering at 1200°C. It can be seen that sintering which occurred could result in microcrack healing and material densification, accompanying with substantial grain growth in some regions.

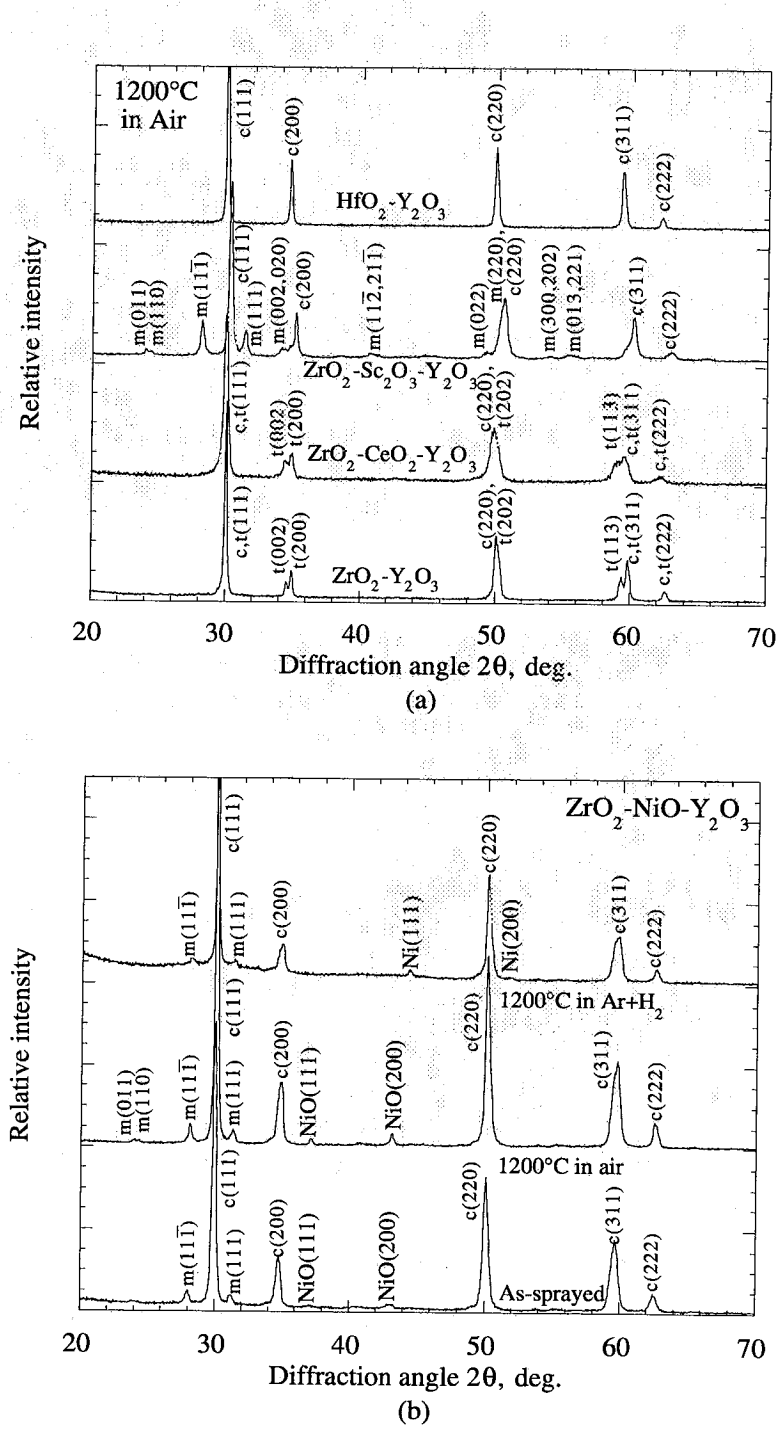

Fig. 6 X-ray diffraction spectra of the plasma-sprayed ceramic coating materials. (a) Diffraction spectra of ZrO_2-Y_2O_3, ZrO_2-CeO_2-Y_2O_3, ZrO_2-Sc_2O_3-Y_2O_3 and HfO_2-Y_2O_3 after 1200°C sintering in air; (b) Diffraction spectra of ZrO_2-NiO-Y_2O_3 under the as-sprayed condition, and after 1200°C sintering in air and 1200°C sintering in Ar+5%H_2.

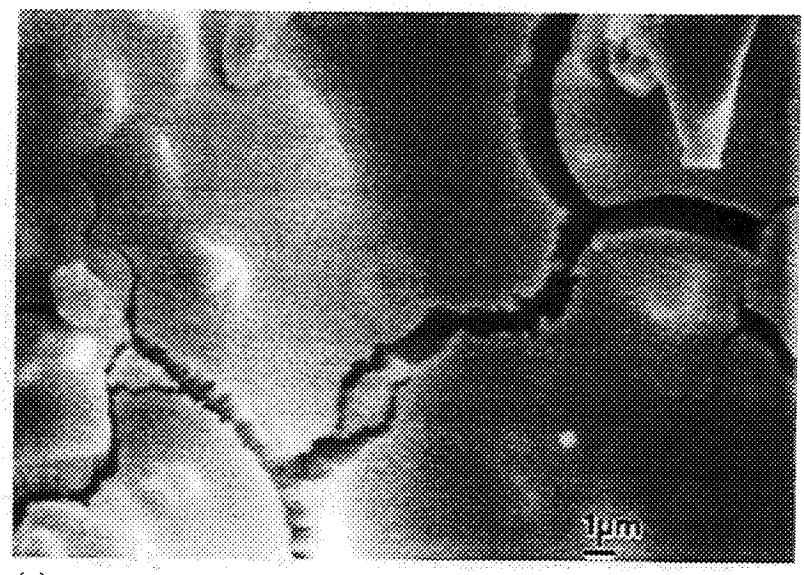

(a)

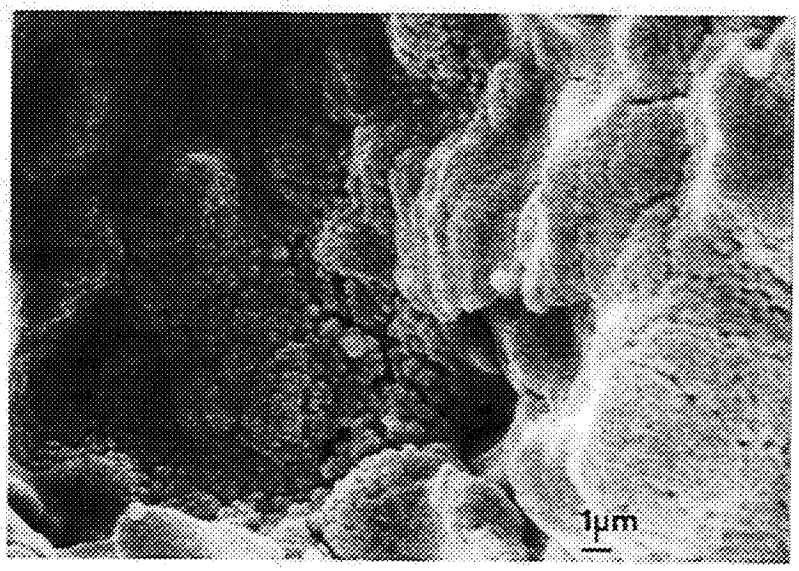

(b)

Fig. 7 Surface micrographs of the ZrO_2-8wt%Y_2O_3 ceramic coating material before and after the dilatometry sintering at 1200°C for 15 hours. (a) Before the sintering test; (b) After the sintering test.

IV. DISCUSSION

The sintering and low-stress creep characteristics of the ceramic coating materials, determined by the dilatometer technique, are similar to the creep behavior of plasma-sprayed coatings obtained from high temperature mechanical creep tests [1, 12, 20] and the laser

sintering/creep test [13]. The fast initial creep rate and low creep activation energy have been attributed to mechanical sliding, fast surface and grain boundary diffusion, and temperature and stress gradient enhanced transport in the porous and weak ceramic coatings [13] . Figure 8 illustrates the creep rates of the plasma-sprayed ZrO_2-8wt%Y_2O_3 as a function of stress and temperature determined by the laser sintering technique [13]. It can be seen that with higher compressive stresses acting on the coating, a long primary creep stage and substantial sintering/creep rates can be observed at much lower temperatures. In the high temperature, low stress sintering/creep tests by the dilatometer technique, mechanical sliding becomes less predominant, and a nearly "steady-state" creep region has been reached in a relatively short period of time. Diffusion-related processes become more important mechanisms for the low stress sintering and creep deformation. The observed grain growth phenomena also suggest the complex diffusion occurring during the dilatometer sintering test.

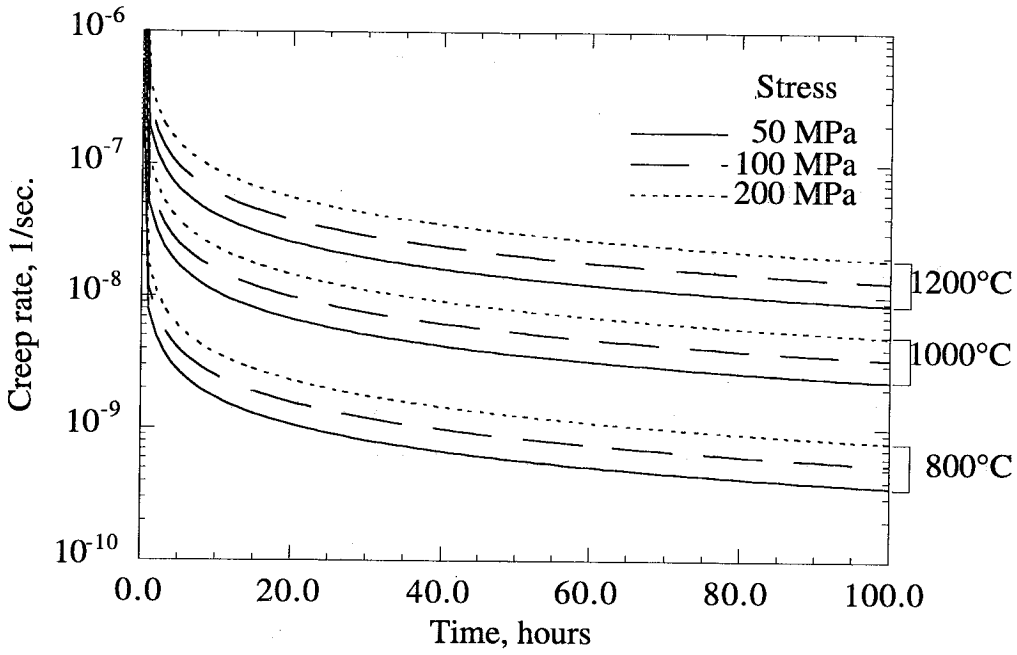

Fig. 8 The coating creep rates of plasma-sprayed ZrO_2-8wt%Y_2O_3, determined by laser high heat flux sintering/creep technique, as a function of stress and temperature.

Creep deformation of ceramic coating materials require diffusion of the cations and anions in these materials. The creep rate in ceramics is therefore determined by the diffusion of the slowest species, diffusing along the fastest path. In yttria-stabilized zirconia, the majority defect types are oxygen vacancies and yttrium aliovalent dopants at normal cation sites. The possible minority defects are zirconia interstitials, zirconium vacancies, and yttrium interstitials, and the zirconium and yttrium cation transport is confirmed to be the slowest process in yttria-stabilized single crystals [21] . The defect reactions in the yttria-stabilized zirconia can be written according to Kröger-Vink notation [22] as

$$Y_2O_3 = 2Y'_{Zr} + 3O_O^{\times} + V_O^{\cdot\cdot} \tag{1}$$

$$O_O^{\times} = V_O^{\cdot\cdot} + 2e' + \frac{1}{2}O_2(g) \tag{2}$$

(for majority defects)

and

$$2O_O^{\times} + Zr_{Zr}^{\times} = Zr_i^{\cdot\cdot\cdot\cdot} + 4e' + O_2(g) \tag{3}$$

$$\frac{1}{2}O_2(g) = V_{Zr}^{''''} + 4h^{\cdot} \tag{4}$$

(for minority defects)

In the extrinsic region, the majority defect oxygen vacancy concentration $\left[V_O^{\cdot\cdot}\right]$ is determined by the dopant yttria concentration $\left[Y'_{Zr}\right]$, which follows the electroneutrality condition

$$\left[Y'_{Zr}\right] = 2\left[V_O^{\cdot\cdot}\right]. \tag{5}$$

At lower oxygen partial pressures in the intrinsic region where the electron conductivity becomes important, oxygen vacancies can be further introduced according to Equation (2), that is

$$\left[V_O^{\cdot\cdot}\right]n^2 = K_{V_O^{\cdot\cdot}} p_{O_2}^{-1/2} \exp\left(-\frac{\Delta H_{V_O^{\cdot\cdot}}}{RT}\right) \tag{6}$$

where n is electron concentration, $K_{V_O^{\cdot\cdot}}$ is reaction constant, $\Delta H_{V_O^{\cdot\cdot}}$ is the enthalpy of formation of oxygen vacancies, R and T are gas constant and temperature, respectively. Metal interstitials can be an important defect type in the oxygen deficient oxide [23] , and the zirconium interstitial concentration can be obtained from Equation (3)

$$\left[Zr_i^{\cdot\cdot\cdot\cdot}\right]n^4 = K_{Zr_i^{\cdot\cdot\cdot\cdot}} p_{O_2}^{-1} \exp\left(-\frac{\Delta H_{Zr_i^{\cdot\cdot\cdot\cdot}}}{RT}\right) \tag{7}$$

where $K_{Zr_i^{\cdot\cdot\cdot\cdot}}$ is a constant, $\Delta H_{Zr_i^{\cdot\cdot\cdot\cdot}}$ is the enthalpy of formation of zirconium interstitials. In this

intrinsic region, the electroneutrality can be expressed as

$$n = 2\left[V_O^{\cdot\cdot}\right] + 4\left[Zr_i^{\cdot\cdot\cdot\cdot}\right]. \tag{8}$$

By combining Equations (6)-(8), the oxygen vacancy and zirconia interstitial concentrations can be written as

$$\left[V_O^{\cdot\cdot}\right] = \left(K_{V_O^{\cdot\cdot}} / 4\right)^{1/3} p_{O_2}^{-1/6} \exp\left(-\frac{\Delta H_{V_O^{\cdot\cdot}}}{3RT}\right) \tag{9a}$$

$$\left[Zr_i^{\cdot\cdot\cdot\cdot}\right] = \left(K_{Zr_i^{\cdot\cdot\cdot\cdot}} / (2K_{V_O^{\cdot\cdot}})^{4/3}\right) p_{O_2}^{-1/3} \exp\left(-\frac{3\Delta H_{Zr_i^{\cdot\cdot\cdot\cdot}} - 4\Delta H_{V_O^{\cdot\cdot}}}{3RT}\right) \tag{9b}$$

(when $\left[V_O^{\cdot\cdot}\right] >> \left[Zr_i^{\cdot\cdot\cdot\cdot}\right]$)

$$\left[V_O^{\cdot\cdot}\right] = \left(K_{V_O^{\cdot\cdot}} / (4K_{Zr_i^{\cdot\cdot\cdot\cdot}})^{2/5}\right) p_{O_2}^{-1/10} \exp\left(-\frac{5\Delta H_{V_O^{\cdot\cdot}} - 2\Delta H_{Zr_i^{\cdot\cdot\cdot\cdot}}}{5RT}\right) \tag{10a}$$

$$\left[Zr_i^{\cdot\cdot\cdot\cdot}\right] = \left(K_{Zr_i^{\cdot\cdot\cdot\cdot}} / 256\right)^{1/5} p_{O_2}^{-1/5} \exp\left(-\frac{\Delta H_{Zr_i^{\cdot\cdot\cdot\cdot}}}{5RT}\right). \tag{10b}$$

(when $\left[V_O^{\cdot\cdot}\right] << \left[Zr_i^{\cdot\cdot\cdot\cdot}\right]$)

In the very high oxygen pressure region where the zirconium vacancies are predominant, the electroneutrality condition can be written as

$$p = 4\left[V_{Zr}^{''''}\right] \tag{11}$$

where p is electron hole concentration. The zirconium vacancy concentration can be obtained from Equation (4) as

$$\left[V_{Zr}^{''''}\right] = \left(K_{V_{Zr}^{''''}} / 256\right)^{1/5} p_{O_2}^{1/10} \exp\left(-\frac{\Delta H_{V_{Zr}^{''''}}}{5RT}\right) \tag{12}$$

where $K_{V_{Zr}^{''''}}$ is a constant, $\Delta H_{V_{Zr}^{''''}}$ is the enthalpy of formation of zirconium vacancies. A Kröger-Vink diagram is constructed based on these defect reactions and Equations (5), (9), (10) and (12), as shown in Figure 9.

The increased sintering rate of ZrO_2-8wt% Y_2O_3 at the reducing Ar+5%H_2 atmosphere is probably related to the defect structure change in the oxide. From the proposed Kröger-Vink diagram shown in Figure 9, it can be seen that both concentrations of oxygen vacancies and zirconia interstitials increase with reducing partial pressure of oxygen, especially in the low oxygen activity region. At extremely low oxygen pressures, the metal cation interstitials can even become the dominant defect type. Therefore, it is possible that the highly defective oxide structures under

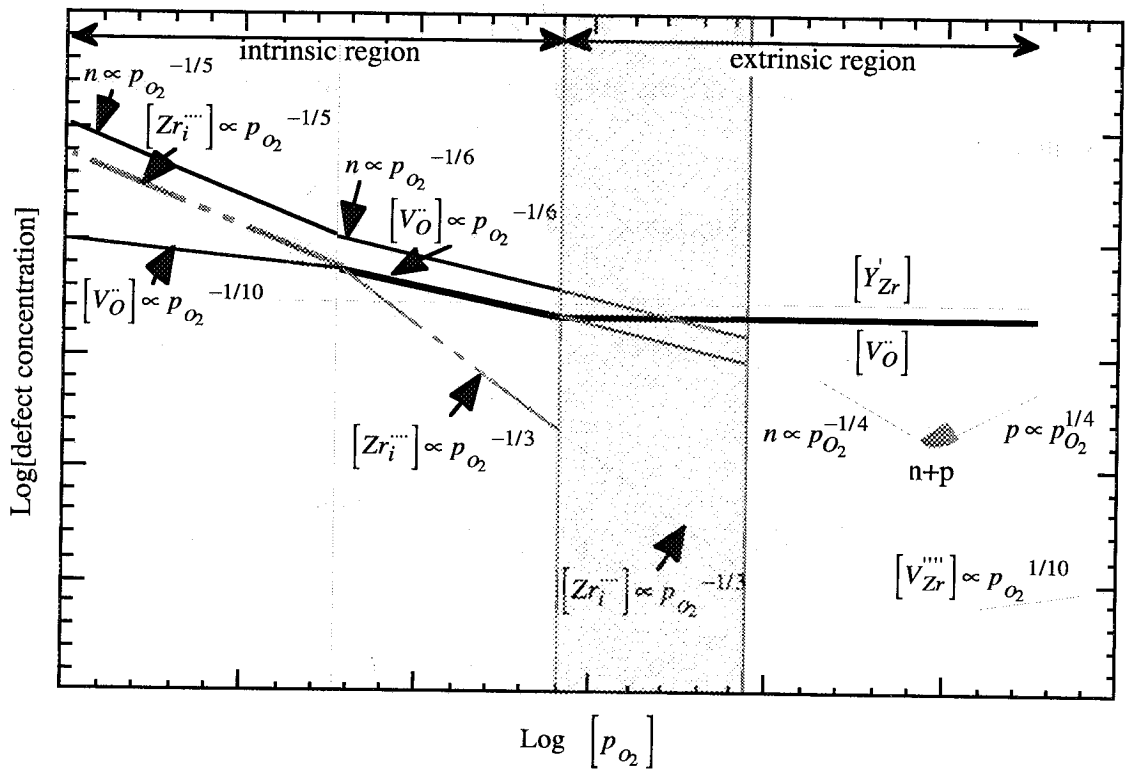

Fig. 9 Proposed Pseudo-Kröger-Vink diagram illustrating the possible majority and minority defects in ZrO_2-8wt%Y_2O_3.

low oxygen pressures facilitates the metal cation interstitial formation, thus resulting in faster metal cation diffusion and the increased sintering rate. Thornton *et al.* [24] have also observed enhanced cerium migration and segregation in the ZrO_2-25wt%CeO_2-2.5wt%Y_2O_3 material under relatively moderate reducing conditions, further confirming the increased cation mobility in more oxygen-deficient oxide under the low oxygen activity conditions.

Since the ceramic sintering requires the transport of the minority cations, the stability of the ceramic materials (both dopants and base materials) will have influence on the sintering behavior. The present study has shown that there is a close relationship between the oxide chemical and phase stability and the sintering rate. Halfnia-based oxides have higher chemical stability, and lower oxygen partial pressures for the transition of ionic conductivity to electronic conductivity, as compared to zirconia-based oxides, therefore it is not surprised that the HfO_2-27wt%Y_2O_3 exhibited the lowest sintering rates. On the other hand, the CeO_2-doped ZrO_2 exhibited large electron contributions at even moderate temperatures and oxygen activities [25]. As shown in Figure 9, the increased region of electron conductivity implies an extended metal cation interstitial

region, in which the cation interstitial concentration is increased with decreasing oxygen partial pressure, and thus resulting in possible enhanced metal cation diffusion with reducing oxygen activity. Insufficient doping, as possibly occurred for Sc_2O_3-doped ZrO_2-Y_2O_3, will have a similar effect on the metal cation diffusion. For the NiO-doped ZrO_2-Y_2O_3, the observed high sintering rates may also be related to NiO segregation at the grain boundaries, which may act as a sintering agent. At lower oxygen partial pressures, the NiO reduction to metallic Ni, as observed in this experiment, can further enhance the sintering process. It is suggested that the chemical and phase stability of both the base oxides and dopant oxides is critical to the sintering and creep behavior of the ceramic materials.

V. CONCLUSIONS

1. Sintering shrinkage strains were observed at the isothermal stage for all ceramic coating materials tested in the dilatometer sintering experiments. The HfO_2-27wt%Y_2O_3 and baseline ZrO_2-8wt%Y_2O_3 exhibited the best sintering resistance, and NiO-doped ZrO_2-Y_2O_3 showed the highest shrinkage strain rates during the tests.
2. The higher shrinkage strain rates of the coating materials were observed for the specimens tested in Ar+5%H_2 as compared to those tested in air. This phenomenon was attributed to a proposed enhanced metal cation interstitial diffusion mechanism under the reducing conditions.
3. There was a close relationship between the observed sintering behavior and chemical and phase stability of the coating materials. Increased chemical stability of base oxides and dopants seems to improve materials phase stability at high temperature, and sintering/creep resistance. Insufficient doping and dopant-segregation-induced depletion will facilitate the sintering process.

REFERENCES

[1] R. F. Firestone, W. R. Logan, J. W. Adams and R. C. J. Bill, in J. D. Buckley, C. M. Packer and J. J. Gebhardt (eds.), The 6th Annual Conference on Composites and Advanced Ceramic Materials, The American Ceramic Society, Inc., Columbus, OH 43214, 1982, p. 758.

[2] R. F. Firestone, W. R. Logan and J. W. Adams, NASA CR-167868, November, 1982.

[3] H. E. Eaton and R. C. Novak, Surface and Coatings Technology, 32 (1987) 227.

[4] T. A. Cruse, S. E. Stewart and M. Ortiz, in (eds.), The Gas Turbine and Aeroengine Congress and Exposition, The American Society of Mechanical Engineers, New York, New York 10017, 1988, p. 1.

[5] S. M. Meier, D. M. Nissely and K. D. Sheffler, NASA CR-182230, July 1991.

[6] H. E. Eaton, J. R. Linsey and R. B. Dinwiddie, in T. W. Tong (eds.), Thermal Conductivity, Lancaster, Pennsylvania, 1994, p. 289.

[7] J. G. Goedjen, W. J. Brindley and R. A. Miller, in C. C. Berndt and S. Sampath (eds.), Advances in Thermal Spray Science and Technology, ASM International, Materials Park, Ohio, 1995, p. 73.

[8] R. B. Dinwiddie, S. C. Beecher, W. Porter, D. and A. B. Nagaraj, in (eds.), The International Gas Turbine and Aeroengine Congress and Exhibition, The American Society of Mechanical Engineers, New York, New York 10017, 1996, p. 1.

[9] D. Zhu and R. A. Miller, Surface and Coatings Technology, 94-95 (1997) 94.

[10] D. Zhu and R. A. Miller, in W. J. Brindley (eds.), The 3rd Thermal Barrier Coating Workshop, sponsored by the TBC Interagency Coordination Committee, NASA Lewis Research Center, Cleveland, Ohio, 1997, p. 139. Materials Science and Engineering, A245 (1998) 212.

[11] K. F. Wesling, D. F. Socie and B. Beardsley, Journal of the American Ceramic Society, 77 (1991) 1863.

[12] G. Thurn, G. A. Schneider and F. Aldinger, Materials Science and Engineering, A233 (1997) 176.

[13] D. Zhu and R. A. Miller, NASA TM-113169, Army Research Laboratory Report ARL-TR-1565, November 1997.

[14] T. A. Cruse, B. P. Johnsen and A. Nagy, Journal of Thermal Spray Technology, 6 (1997) 57.

[15] S. R. Choi, D. Zhu and R. A. Miller, in (eds.), International Symposium on Advanced Synthesis and Processing, The 22nd Annual Conference on Composites and Advanced Ceramic Materials, 1998.

[16] R. A. Miller and G. W. Leissler, NASA TP-3296, March 1993.

[17] S. Chen and P. Shen, Materials Science and Engineering, A123 (1990) 145.

[18] R. L. Jones, R. F. Reidy and D. Mess, Surface and Coatings Technology, 82 (1996) 72.

[19] D. Zhu and R. A. Miller, NASA Technical Paper TP-3676, Army Research Laboratory Technical Report ARL-TR-1341, May 1997.

[20] B. P. Johnsen, T. A. Cruse, R. A. Miller and W. J. Brindley, Journal of Engineering Materials and Technology, 117 (1995) 305.

[21] H. Solmon, J. Chaumont, C. Dolin and C. Monty, in T. O. Mason and J. L. Routbort (eds.), Ceramic Transactions - Point Defects and Related Properties of Ceramics, The American Ceramic Society, Inc, Westerville, Ohio, 1991, p. 175.

[22] F. A. Kröger, The Chemistry of Imperfect Crystals, North-Holland Publishing Company., Amsterdam, 1964.

[23] P. Kofstad, Nonstoichiometry, Diffusion, and Electrical Conductivity in Binary Metal Oxides, Robert E. Krieger Publishing Company, Malabar, Florida, 1983.

[24] J. Thornton, A. Majumdar and G. AcAdam, Surface and Coatings Technology, 94-95 (1997) 112.

[25] R. F. Reidy and G. Simkovich, Solid State Ionics, 62 (1993) 85.

REPORT DOCUMENTATION PAGE

Form Approved
OMB No. 0704-0188

1. AGENCY USE ONLY (*Leave blank*)	2. REPORT DATE	3. REPORT TYPE AND DATES COVERED
	July 1998	Technical Memorandum

4. TITLE AND SUBTITLE

Sintering and Creep Behavior of Plasma-Sprayed Zirconia and Hafnia Based Thermal Barrier Coatings

5. FUNDING NUMBERS

WU–505–23–2U–00

6. AUTHOR(S)

Dongming Zhu and Robert A. Miller

7. PERFORMING ORGANIZATION NAME(S) AND ADDRESS(ES)

National Aeronautics and Space Administration
Lewis Research Center
Cleveland, Ohio 44135–3191

8. PERFORMING ORGANIZATION REPORT NUMBER

E–11239

9. SPONSORING/MONITORING AGENCY NAME(S) AND ADDRESS(ES)

National Aeronautics and Space Administration
Washington, DC 20546–0001

10. SPONSORING/MONITORING AGENCY REPORT NUMBER

NASA TM—1998-208406

11. SUPPLEMENTARY NOTES

Prepared for the 25th International Conference on Metallurgical Coatings and Thin Films sponsored by the American Vacuum Society, San Diego, California, April 27—May 1, 1998. Dongming Zhu, Ohio Aerospace Institute, 22800 Cedar Point Rd., Cleveland, Ohio 44142, and Robert A. Miller, NASA Lewis Research Center. Responsible person, Dongming Zhu, organization code 5160, (216) 433–5422.

12a. DISTRIBUTION/AVAILABILITY STATEMENT

Unclassified - Unlimited
Subject Category: 27 Distribution: Nonstandard

This publication is available from the NASA Center for AeroSpace Information, (301) 621–0390.

12b. DISTRIBUTION CODE

13. ABSTRACT (*Maximum 200 words*)

The sintering and creep of plasma-sprayed ceramic thermal barrier coatings under high temperature conditions are complex phenomena. Changes in thermomechanical and thermophysical properties and in the stress response of these coating systems as a result of the sintering and creep processes are detrimental to coating thermal fatigue resistance and performance. In this paper, the sintering characteristics of ZrO_2-8wt%Y_2O_3, ZrO_2-25wt%CeO_2-2.5wt%Y_2O_3, ZrO_2-6w%NiO-9wt%Y_2O_3, ZrO_2-6wt%Sc_2O_3-2wt%Y_2O_3 and HfO_2-27wt%Y_2O_3 coating materials were investigated using dilatometry. It was found that the HfO_2-Y_2O_3 and baseline ZrO_2-Y_2O_3 exhibited the best sintering resistance, while the NiO-doped ZrO_2-Y_2O_3 showed the highest shrinkage strain rates during the tests. Higher shrinkage strain rates of the coating materials were also observed when the specimens were tested in Ar+5%H_2 as compared to in air. This phenomenon was attributed to an enhanced metal cation interstitial diffusion mechanism under the reducing conditions. It is proposed that increased chemical stability of coating materials will improve the material sintering resistance.

14. SUBJECT TERMS

Thermal barrier coatings; Ceramic sintering and creep; Defect structure; Dilatometry

15. NUMBER OF PAGES

23

16. PRICE CODE

A03

17. SECURITY CLASSIFICATION OF REPORT	18. SECURITY CLASSIFICATION OF THIS PAGE	19. SECURITY CLASSIFICATION OF ABSTRACT	20. LIMITATION OF ABSTRACT
Unclassified	Unclassified	Unclassified	